Chapter 5: Prediction of Barium Sulfate Deposition in Petroleum and Hydrothermal Systems

Derek M. Hall [a,b,c], Serguei N. Lvov [a,b,c], Isaac K. Gamwo[a]

[a]U.S. Department of Energy, National Energy Technology Laboratory, Research & Innovation Center, Pittsburgh, PA 15236, USA

[b]Department of Energy and Mineral Engineering, The Pennsylvania State University, University Park, PA 16802, USA

[c]The EMS Energy Institute, The Pennsylvania State University, University Park, PA 16802, USA

Abstract

Precipitation of minerals such as barium sulfate in production equipment and within reservoirs in petroleum and other hydrothermal producing (e.g. geothermal) systems is a major operational problem. Barium sulfate deposition can cause different problems such as loss in production, formation damage and premature equipment failure. Mineral deposition is usually caused by changes in the producing fluid temperature or composition and chemistry. In these systems, aqueous systems thermodynamic modeling plays a central role in predicting the favorability of barite precipitation and dissolution. Predominance diagrams and speciation models demonstrate how solution properties such as pH and electrolyte composition impact the solubility limit of barite. Temperature and pressure have a strong influence on barite solubility. The solubility limit of barite varies from 5 to 25 μmol kg^{-1} depending on the temperature. Commercial software such as OLI Studio that relies on the Helgeson-Kirkham-Flowers (HKF) equation of state model (EOS) present disclaimers that the model does not

work at high temperatures and low pressures above 300 °C [1]. Here, we present a model that is able to predict the behavior of barite-containing species at high temperatures and pressures. This was accomplished using a molecular statistical thermodynamic-based model capable of predicting the solubility of barite beyond the critical point of water. The resulting predictions accurately captured increases in solubility from 0 - 100 °C, decreases in solubility from 100 to 300 °C and then a steady increase to 400 °C which covers the range of temperatures currently being explored by hydrothermal and petroleum systems.

5.1 Mineral Deposition in Petroleum and Hydrothermal Systems

Mineral deposition is a critical problem facing engineers working with petroleum and hydrothermal fluids. These problems are most apparent for petroleum and natural gas (PNG) industry and geothermal systems. If left unchecked, hydrothermal fluids can quickly become supersaturated and form mineral deposits that damage the productivity of a production field. As recent explorations have dramatically expanded the range of temperatures and pressures observed in PNG and geothermal reservoirs, we need to adapt our current modelling practices to capture these new conditions.

The process of forming these deposits is referred to as scaling, which affects the productivity of many geoengineered systems. One extreme example of a detrimental scaling incident occurred in the Miller oilfield in the North Sea. When an oil well went from 30,000 barrels per day of production to zero within 24 hours [2]. The cause of the production shutdown was a mineral plug of barium sulfate (barite) several hundred feet long which had quickly formed within the well [2].The Miller oilfield scaling incident is a classic example of how the scaling phenomena can adversely impact production from conventional oil fields, but this is just one instance as several other examples can be found throughout literature [3–7]. Scaling is also a possible cause of the rapid production drop-off observed in unconventional oil and gas fields. Though the use of hydraulic fracturing has played a critical role in the

resurgence of oil and gas exploration in shale reservoirs, these unconventional fields are known for their rapid decrease in production over time [8,9]. Here is a typical plot of the production decline from unconventional reservoirs showing the hyperbolic decline and exponential tail decline phases (Figure 5.1) [10].

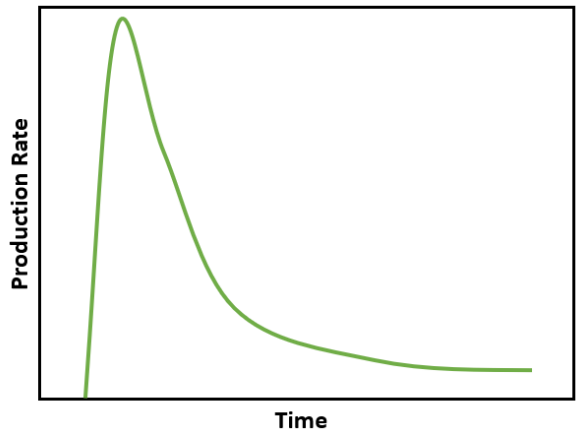

Figure 5.1: Typical sketch production profile from unconventional well.

Their use of acidic and often complex hydraulic fracturing fluids (HFFs) aim to enhance the transport properties, increasing reservoir productivity. However, these reservoirs are subject to injection sequences which introduce the HFFs into the reservoir then undergo extended shut-in periods which neutralize the incoming fluids through their contact with minerals and fluids contained within the formation [8]. Recent studies have shown that mineral precipitation within these reservoirs, as well as deposits inside fractures, near pore throats and at the surface of proppant materials, leads to reduced porosities. [11]. Minerals found within the fracture network consist of species such as Fe(III)-containing solids, calcite and barite [8,9,11].

Scaling occurs in environments that share some core commonalities. In a hydrothermal system, scaling occurs if an aqueous solution becomes supersaturated with ions that contain the elements needed to form a mineral such as barite or calcite. In principle, a solution can either be saturated, undersaturated or supersaturated with a mineral depending on the activity

of mineral constituents within the aqueous phase. In these circumstances, specific outcomes are expected. Supersaturated solutions deposit minerals, undersaturated solutions dissolve minerals, and saturated solutions will neither dissolve or deposit a mineral as they are in equilibrium with these solid mineral phases. The solubility limit, which determines each of these states is a thermodynamic property. Kinetics of deposition/dissolution could impact the rate of these processes but their thermodynamics provides the principle possibility of these processes to occur.

The extent of mineral saturation in any solution can be determined through a thermodynamic analysis of the solid and aqueous phase. Through such an analysis, concepts such as scaling tendency, saturation index (sometimes called the scaling index) and solubility products are used to assess if deposition is thermodynamically favorable. One common mineral known to cause scaling issues is barite. Here, barite precipitation and dissolution are described using the International Union of Pure and Applied Chemistry (IUPAC) conventions [12]:

$$BaSO_4(s) \leftrightarrow Ba^{2+}(aq) + SO_4^{2-}(aq). \quad (5.1)$$

$BaSO_4(s)$ represents the mineral barite in its solid phase "(s)", and $Ba^{2+}(aq)$ and $SO_4^{2-}(aq)$ are the barium and sulfate charged species (ions) present in an aqueous phase "(aq)". In addition to the ionic species, ion pairs such as $BaSO_4^0(aq)$, can also form within the aqueous phase and are critical to understanding barite solubility in superheated waters as the attraction between ions increases due to decrease of relative permittivity (dielectric constant) of water. Formation of the ion pairs and other complexes is a common phenomenon for any strong electrolyte when temperature of solution increases and its density decreases. This formation of ion pairs and complexes needs to be considered in modelling and predicting mineral

deposition in petroleum and hydrothermal systems at high temperatures and low pressures.

5.2 Solubility Product Constants and Scaling Tendencies

Knowing the saturation limit of barite in a solution is a useful tool for predicting its likelihood of deposition. The solubility product constant (K_{sp}), also called the solubility product, is an equilibrium constant (K_{eq}) for a mineral dissolution reaction such as the one shown in **Eq. 5.1** and provides a means of quantifying this limit. Like all equilibrium constants, they can be determined from standard Gibbs energy of reaction ($\Delta_r G^0$) values as follows:

$$\ln(K_{eq}) = -\Delta_r G^0 \ (RT)^{-1}, \tag{5.2}$$

where R is the molar gas constant (in J mol^{-1} K^{-1}) and T is the thermodynamic temperature (in K). Alternatively, K_{eq} can be expressed in terms of activities. For barite dissolution, K_{sp} is as follows:

$$K_{sp} = a_{Ba^{2+}(aq)} a_{SO_4{}^{2-}(aq)} / a_{BaSO_4(s)}, \tag{5.3}$$

where $a_{Ba^{2+}(aq)}$ is the activity of barium ions, $a_{SO_4{}^{2-}(aq)}$ is the activity of sulfate ions and $a_{BaSO_4(s)}$ is the activity of barite which is equal to 1 for pure mineral.

The ion activity product (IAP), also known as Q in some texts, $a_{Ba^{2+}(aq)} \times a_{SO_4{}^{2-}(aq)}$, of a solution is key indicator of whether a solution is capable of precipitating barite. The ratio of IAP and K_{sp} is also used in predicting scaling tendencies:

$$\Omega = \text{IAP}\ K_{sp}^{-1} \tag{5.4}$$

where Ω, the ratio of IAP and K_{sp}, is referred to as the scaling tendency and is used to assess the favorability of barite deposition from a solution [13]. As such, if a solution with an IAP of barium $a_{SO_4{}^{2-}(aq)}$ions is ever greater than its K_{sp}, then that solution is supersaturated with respect to barite. Conversely, solutions with an IAP lower than K_{sp} are undersaturated and will dissolve the mineral. However, we should note that thermodynamic values only tell us if precipitation and dissolution can happen. Kinetics of these reactions should be considered to determine if they happen in any meaningful timeframe.

Therefore, by calculating the $\Delta_r G^0$ using **Eq. 5.1**, we can assess the favorability of barite deposition in a given solution. The $\Delta_r G^0$can be calculated for **Eq. 5.1** as follows:

$$\Delta_r G^0 = \Delta_f G^0_{\mathrm{Ba^{2+}(aq)}} + \Delta_f G^0_{\mathrm{SO^{2-}}(aq)} - \Delta_f G^0_{BaSO_4(s)} \ , \tag{5.5}$$

where ΔG_i^0 is the standard Gibbs energy of formation of the i-th chemical in the reaction (eq. 5.5). The standard Gibbs energy of formation does not depend on concentration, but it does depend on the concentration scale. The concentration scales used with aqueous systems are molality (b), molarity (c) and mole fraction (x). Briefly, molality is defined as mol of solute per 1 kg of water, whereas molarity is mol of solute per 1 L of solution. Mole fraction is a dimensionless value that is the ratio of the number of moles of one component of a solution (solute or solvent) to the total number of moles representing all of the solution components. Comparing standard values in literature can be confusing because these concentration scales are rarely reported, but often lead to ~10 kJ mol^{-1} differences between sources. For reliable calculations, the origins of the standard Gibbs energy values should be carefully considered before use. The SUPCRT92 database [14] is a great starting point for many systems as it is internally consistent amongst its many species and valid for a sizable range of temperatures

and pressures. As an example, we will calculate $\Delta_r G^0$ for barite precipitation at 25 °C and 1 bar as

$$\Delta_r G^0 = \Delta_f G^0_{\mathrm{Ba^{2+}(aq)}} + \Delta_f G^0_{\mathrm{SO^{2-}}(aq)} - \Delta_f G^0_{BaSO_4(s)}$$

$$= (-560.8 \text{ kJ mol}^{-1}) + (-744.5 \text{ kJ mol}^{-1}) - (1{,}362.1 \text{ kJ mol}^{-1}) = 56.92 \text{ kJ mol}^{-1}.$$

With the $\Delta_r G^0$ known, the natural logarithm of the solubility product for barite at 25 °C and 1 bar can be readily calculated as:

$$\ln(K_{sp}) = -\Delta_r G^0 (RT)^{-1}$$

$$= -(56{,}916 \text{ J mol}^{-1}) / [(8.3145 \text{ J mol}^{-1}\text{K}^{-1})(298.15 \text{ K})]$$

$$= -22.96,$$

resulting in a K_{sp} of 1.069×10^{-10}. If the solution only contains barium ions, sulfate ions and water, then the square root of K_{sp} provides a means to estimate the solubility limit of barite in water [$(1.069 \times 10^{-10})^{0.5} = 1.034 \times 10^{-5}$ mol kg^{-1} at 25 °C and 1 bar]. The solubility limit we calculated here is consistent with the 1.11×10^{-5} (± 8 %) mol kg^{-1} obtained experimentally [15].

Note that in the above calculations we assumed that the activity coefficients of aqueous species equal 1, so activity of the i-th species, a_i, is numerically the same as molal concentration, b_i, while precisely $a_i = b_i/b^0$, where b^0 is the standard molality equals 1 mol/kg, so the activity is dimensionless.

The introduction of activity and activity coefficients bring up some important concepts about the relationship between concentration and activity. As the concentration of

ions in a solution increases, interactions between these ions alter the effective concentration of each species, which we call activity. The deviation due to these interactions are accounted for through activity coefficients, which are obtained using a wide variety of equations that are thoroughly explained elsewhere [13]. As many geochemical fluids contain a plethora of ions, these deviations can be dramatic depending on the conditions. Likewise, minerals can form solid solutions which also require careful treatment. Though we acknowledge these factors and their significance, this chapter will focus on how composition (excluding activity coefficient effects) and temperature impact barite precipitation predictions. Excluding the activity coefficients considering very dilute solutions is a reasonable approximation.

In many instances, Ω can vary by several orders of magnitude, so another metric is used to quantify the likelihood of barite and other minerals to precipitate from a solution. The saturation index (SI), which is defined as $SI = \log_{10}(\Omega)$, can provide a similar assessment of the likelihood whether a mineral will dissolve or precipitate in the given solution [13]. An SI equal to zero means the solution is at equilibrium with the mineral in question, while a negative SI indicates the mineral is predicted to dissolve and a positive SI means that the mineral is predicted to precipitate. These perditions are based on thermodynamics and the precipitation/dissolution kinetics should also be taken into account in some cases.

5.3 Speciation Models and Predominance Diagrams

The solubility product can make the prediction of barite scaling seem deceptively simple. However, the presence of additional species complicates scaling thermodynamics as they can influence the maximum solubility sulfate and/or barium-containing species. Such complications are frequent in real world applications as engineers regularly work with natural and produced waters with a diverse range of components. The injection of produced waters [4] or seawater [2,5,6] into the reservoir to enhance oil recovery can increase the

concentration of ionic species within the reservoir that can promote the formation of mineral scale. For example, pH, temperature and fluid density variations can favor the formation of additional barium-containing species such as the barium hydroxide complex, e.g. $BaOH^{+}(aq)$, or the ion-pair, e.g. $BaSO_4^0(aq)$ [16]. Problems such as these can be solved by developing a more realistic speciation model.

Speciation analysis is an approach that quantifies the thermodynamically favorable phases and their components (molecules, ions, ion pairs, etc.) for a particular system at particular state variables such as temperature and pressure. With respect to barite mineral scaling, speciation analysis can provide insights into how the chemical composition of produced waters can influence solubility of barite. The effects of dissolved salts, gases and pH as well as temperature and pressure can be analyzed through this approach. As produced waters have a wide range of chemical and physical properties [4,17], speciation analysis is often needed to discern the fate of any mineral components within the production lines.

Two methods are commonly used to examine the speciation of a petroleum and hydrothermal system which shows how solution composition and the solubility limit of minerals can change in response to additional chemicals. The first relies on solving a system of equilibrium constants along with equations of electroneutrality and mass balance and the second relies on minimizing the Gibbs energy of the system [13, 18]. The equilibrium constant method relies on identifying chemicals reactions that represent a system of interest, while the minimization method requires all Gibbs energies of formation of all species are available. In addition to the barite dissolution reaction shown in **Eq. 5.1**, barium hydroxide species is another well-known barium-containing aqueous species. Changing pH of the solution using acids and bases can invoke a wide range of responses. The chemicals used to change the system pH, will strongly influence the outcome. Adjustments to pH invoke sulfate reactions involving protons as well as sulfate ions and hydrogen sulfate which can

influence the solubility of barium sulfate significantly. Furthermore, a barium sulfate ion-pair, $BaSO_4^0(aq)$, can impact solubility at higher temperatures particularly in the presence of sulfate-containing electrolytes [16,19,20]. These relations can be expressed using additional chemical reactions:

$$BaOH^+(aq) \leftrightarrow OH^-(aq) + Ba^{2+}(aq), \quad (5.6)$$

$$HSO_4^-(aq) \leftrightarrow SO_4^{2-}(aq) + H^+(aq), \quad (5.7)$$

$$H_2O(l) \leftrightarrow H^+(aq) + OH^-(aq), \quad (5.8)$$

$$BaSO_4^0(aq) \leftrightarrow Ba^{2+}(aq) + SO_4^{2-}(aq). \quad (5.9)$$

Using **Eq. 5.2** and the SUPCRT92 database as well as some published ion-pair data [16,19,20], K_{eq} values for each of these reactions can be calculated for a wide range of temperatures and pressures. As shown in Table 5.1, at 25 °C and 1 bar, the K_{eq} values for each of these reactions can be different by more than 30 orders of magnitude.

Table 5.1: Overview of chemical reactions and equilibrium constants for **Eqs. 5.1 & 5.6-5.9** at 25 °C and 1 bar.

Chemical Reactions	**ln(K_{eq})**
$K_1: BaSO_4(s) \leftrightarrow Ba^{2+}(aq) + SO_4^{2-}(aq)$	-22.96
$K_2: BaOH^+(aq) \leftrightarrow OH^-(aq) + Ba^{2+}(aq)$	-1.14
$K_3: HSO_4^-(aq) \leftrightarrow SO_4^{2-}(aq) + H^+(aq)$	-4.56
$K_4: H_2O(l) \leftrightarrow H^+(aq) + OH^-(aq)$	-32.22

$$K_5 : BaSO_4^0(aq) \leftrightarrow Ba^{2+}(aq) + SO_4^{2-}(aq) \qquad -6.14$$

If combined with mass balance and charge balance constraints, these equations form a system of equations that provide a means to determine the molal concentration (b_i) of all species within an aqueous phase. Here is a demonstration of how these can be solved assuming the activity coefficients (γ_i) are close to 1 (i.e. $a_i = b_i\gamma_i \approx b_i$), which is only applicable in very dilute solutions [21]. Otherwise, an iterative approach is required to account for how activity coefficients change with the ionic strength of the solution, which is an approach presented elsewhere [13].

The K_{eq} equations for K_1-K_5 can be expressed in terms of activities (using square brackets) according to **Eqs. 5.10-5.14:**

$$K_1 = [b_{Ba^{2+}}][\, b_{SO_4^{2-}}], \tag{5.10}$$

$$K_2 = [b_{Ba^{2+}}][\, b_{OH^-}] \,/\, [b_{BaOH^+}]\,, \tag{5.11}$$

$$K_3 = [b_{SO_4^{2-}}][\, b_{H^+}] \,/\, [b_{HSO_4^-}]\,, \tag{5.12}$$

$$K_4 = [b_{OH^-}][\, b_{H^+}]\,, \tag{5.13}$$

$$K_5 = [b_{Ba^{2+}}][\, b_{SO_4^{2-}}] \,/\, [b_{BaSO_4^0}]\,. \tag{5.14}$$

By selecting a pH titrant concentration and the total amount of moles of barium per kg of water for a system ($b_{total,Ba}$), we can solve the system of equations to determine solubility of barium sulfate at a given pH by including the following mass balance and charge balance equations, **Eq. 5.15** and **Eq. 5.16** if we assume the counterions do not require additional

reactions to be considered:

$$b_{total,Ba} = b_{Ba^{2+}} + b_{BaSO_4^0} + b_{BaSO_4(s)} + b_{BaOH^+}, \quad (5.15)$$

$$0 = 2b_{Ba^{2+}} + b_{BaOH^+} + b_{H^+} - b_{OH^-} - b_{HSO_4^-} - 2\, b_{SO_4^{2-}} + b_{Na+}. \quad (5.16)$$

We set the total barium sulfate in the system to be 0.1 mol per kg of water, and we set the pH of the system and the counter ion concentration. If the titrants are NaOH and H_2SO_4, a parametric sweep of pH shows an increase in the solubility of barium sulfate from acidic to neutral conditions and a plateau at high pH (Figure 5.2.A). The lower solubility at low pH is due to the higher concentrations of sulfate ions from the addition of the sulfuric acid to decrease the pH. (Figure 5.2.B)

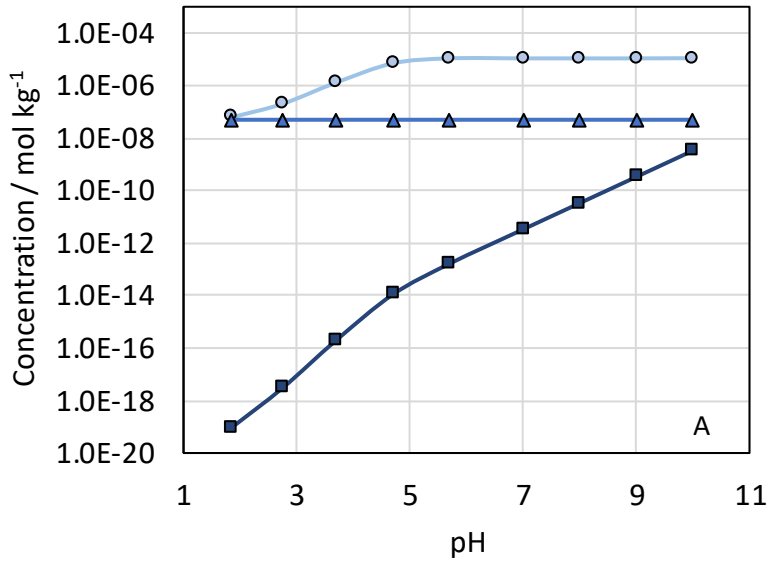

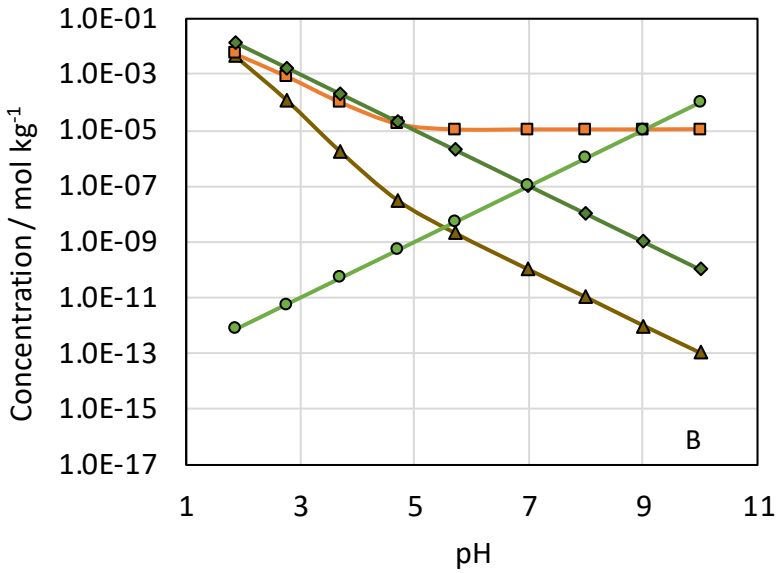

Figure 5.2: Predominance diagrams for (A) barium-containing species and (B) non-barium containing species at 25 °C and 1 bar for a $BaSO_4$ - H_2O system. The titrants were NaOH and H_2SO_4. For pH 7 and higher, $b_{Na+(aq)} = b_{OH-(aq)}$. ($b_{Ba^{2+}}$= ○, b_{BaOH^+}= ■, $b_{BaSO_4^0}$ = △, b_{H^+} = ♦, b_{OH^-} = ●, $b_{HSO_4^-}$ = ▲, $b_{SO_4^{2-}}$ = □)

The approach presented in this section demonstrates how speciation models and predominance diagrams can be used to visualize solubility and scaling trends for barite as a function of the solution chemistry change. Similar diagrams can be developed for a number of compositional changes such as variations in sulfate and chloride concentrations. These diagrams can also be configured for a range of temperatures and pressures to study their influence on barite solubility. However, the equilibrium constant method becomes increasingly difficult as the number of species and possible reactions increase. For example, if we used HCl instead of H_2SO_4 to control the pH, then reactions with barium chloride are needed otherwise erroneous results will be obtained. For more complex systems with multiple phases and multiple components such as examples given in Refs. [22–24], Gibbs energy minimization using a commercial software is a more convenient approach.

5.4 Barium Sulfate Solubility Measurements at Elevated Temperatures and Pressures

Solubility of barite is generally quite low which often results in scaling. At saturated pressures, P_{sat}, the solubility increases to around 100 ^{o}C, then it decreases in a temperature range between 100 and 300 ^{o}C. From 25 to 300 °C, increasing pressure from 10 to 100 MPa increases the barite solubility [16]. A few techniques were used for measuring barite solubility such as liquid phase sampling in autoclave and flow systems, weight loss of crystal, conductivity, spectroscopy, liquid scintillation, X-ray fluorescence, inductively coupled plasma-atomic emission spectroscopy, sulfur radioactive tracer, and barium radioactive tracer.

In Ref. [15] the solubility data of barite in pure water for a temperature range between 0 and 300 ^{o}C at P_{sat} was collected from 29 publications (Figure 5.3).

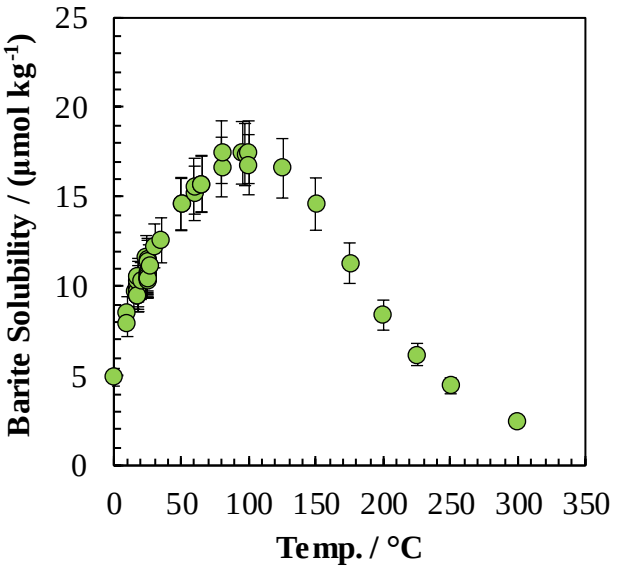

Figure 5.3: Experimental solubility data for barite in water at P_{sat} as a function of temperature. (Based on Krumgalz et al. 2018 [15])

In Ref. [15], the data were carefully evaluated and fitted to the following polynomial equation:

$$b = \alpha_0 + \alpha_1 t + \alpha_2 t^2 + \alpha_3 t^3 , \quad (5.17)$$

where b is barite solubility in mol per 1 kg of water (molality), t is temperature in degrees Celsius and the parameters a_i were estimated as:

$\alpha_0 = 5.176\ 10^{-6}$ mol/kg ,

$\alpha_1 = 2.852\ 10^{-7}$ mol/(kg ^{o}C) ,

$\alpha_2 = -2.024\ 10^{-9}$ mol/(kg ^{o}C^2) ,

$\alpha_3 = 3.473\ 10^{-12}$ mol/(kg ^{o}C^3).

Using 47 experimental points with $R^2 = 0.983$ it was observed that discrepancies between the experimental solubilities and those calculated by this polynomial are below 4.34 %.

Solubility data for barite in pure water at temperatures above 300 ^{o}C were presented and discussed in a reference book [25]. Morey and Hesselgesser [26] measured $BaSO_4$(s) solubility at 500 ^{o}C and 1000 bar using a flow method to pass supercritical water at a constant pressure over the mineral with the fluid exiting the system being analyzed to assess the solubility. Their measurement error is uncertain as it is not reported or listed. Strübel studied barite solubility in water at three conditions: temperature range of 200-600 ^{o}C and pressures of 15.6-2100 bar; isobaric conditions and densities of 0.326-0.925 g/cm^3; isochoric conditions using a weight loss of crystal method [27]. The authors provided an uncertainty of the solubility measurements of ± 20-25 %. Gundlach et al. [28] applied a method of liquid

phase sampling taken from a high temperature autoclave with following analysis of the sample. The covered temperature and pressure ranges were 200-350 ^{o}C and 15.9-168.6 bar. Their measurement error is uncertain as it is not reported or listed. Blount carried out the $BaSO_4$ solubility measurements [29] using hydrothermal equipment previously described in Ref. [30]. A method for sampling the liquid phase was developed to avoid corrosion and achieve equilibrium in the aqueous phase. The studies were done at temperatures 189-279 ^{o}C and pressures 92-1010 bar. Their measurement error is also uncertain as it is not reported. Therefore, while a few barite solubility studies were carried out at temperatures above 300 ^{o}C, precision and reliability of the generated data were not well-defined. Given that Blount and Strübel contradict each other by a factor of 2 to 5 in regions they overlap, more solubility measurements are needed to confirm the Strübel dataset.

5.5 Thermodynamic Model for Aqueous Species at High Temperatures and Pressures

Here we present how a new aqueous thermodynamic model can be used to predict solubilities for a wide range of temperatures and pressures. The widely accepted equation of state that is used to predict the solubility of minerals from room temperature up to elevated temperatures is not suitable in many high-temperature, high-pressure (HTHP) conditions. Computational software and databases, such as the SUPCRT92 database, rely on the Helgeson-Kirkham-Flowers (HKF) model. The SUPCRT database and HKF model can reliably predict the solubility of barite up to 300 °C. However, this model does not include data related to the ion-pair $BaSO_4$, which is a major contributor to the solubility predictions at higher temperatures and pressures. In their seminal works, the authors of the HKF model indicate that their model fails at high temperatures (> 300 °C) and low fluid densities (< 0.8 g cm^{3}) [14,31,32]. Though oil and gas applications do reach these temperatures, geothermal systems more frequently operate in this region [33]. As such, even if we were to fit the ion pair, the

HKF model is unable to reliably predict the solubility limits of barite for some hydrothermal systems even though it could in principle work at high temperatures if the fluid density is large enough. A demonstration that SUPCRT does not work at temperatures > 300 °C is given below were the calculated by SUPCRT and experimental values of $BaSO_4$ solubility are compared.

Recent advancements in molecular statistical thermodynamics (MST) relating to molecular interactions can provide a more reliable description of how the standard Gibbs energy of solute molecules vary with temperature and pressure [31,34,35]. Previous works have shown that dipole-dipole and ion-dipole statistical thermodynamic expressions improve the predictive capabilities of standard thermodynamic models to a broader range of conditions [31,32]. Mineral solubility and ion-pair association reactions ($NaOH^0$, HCl^0, KCl^0) with available experimental data were used to confirm the viability of this new approach for extending the range of solubility predictions beyond those set by the landmark HKF model [18,31,32,36].

Like the HKF model, this approach predicts the apparent standard molar Gibbs energy of formation for aqueous species. Note that the apparent Gibbs energy of formation differs from "typical" standard Gibbs energy of formation in that the standard Gibbs energy of species in their elemental form are only zero at 25 °C and 1 bar. For example, molecules such as $H_2(g)$ will have non-zero apparent standard Gibbs energy values at elevated temperatures and pressures. Like the HKF model, the proposed MST-supported model uses the following equation:

$$\Delta G^0_j(T, P) = \Delta_f G^0_j(T_r, P_r) + [\, G^0_j(T, P) - G^0_j(T_r, P_r)] \,, \tag{5.18}$$

to determine the apparent standard Gibbs energy, $\Delta G^0_j(T, P)$, of the j-th species at given

temperature (T) and pressure (P). Here, $\Delta_f G^0_j(T_r,P_r)$ is the standard Gibbs energy of the j-th species at the reference temperature of 25 °C and pressure of 1 bar, and [$G^0_j(T, P) - G^0_j(T_r, P_r)$] is the change in the standard partial molar Gibbs energy of the j-th species from changes in T and P. The second term is determined using a series of expressions that depend on temperature, pressure, properties of pure water and five fitting parameters:

$$G^0_j(T, P) - G^0_j(T_r, P_r) = [\sum_k S_j^k(T_r, P_r) - S_j^0(T_r, P_r)](T - T_r) + A_j(P - P_r) - C_j\left(T ln \frac{T}{T_r} + T_r - T\right) + (\sum_k G_j^k(T, P) - \sum_k G_j^k(T_r, P_r)) \ . \quad (5.19)$$

The G_j^k terms are the MST-based k-type partial molar Gibbs energy contributions which include the hard sphere (HS) contributions, the electrostatic ion-dipole (ID) and dipole-dipole (DD) contributions, reference state contributions for changes in the standard state density (SS) and Gibbs energy changes for switching from unit mol fraction to unit molality reference states (MS). The model includes entropy terms for each of these contributions (S_j^k), which can be determined by taking the derivative of each contribution with respect to temperature, and the standard partial molar entropy at the reference point (S_j^0). These were reported previously [31]. Lastly, A_j and C_j are two empirical constants used to account for the short-range interactions. The remaining three of the five fitting parameters are within the MST expressions used to determine the G_j^k terms.

Three MST expressions represent the bulk of the temperature and pressure dependences. The remaining fitting parameters within these expressions are σ_i, σ_w, and p_j that are the ion/ion pair diameter, water molecule diameter and ion pair dipole moment, respectively. The hard sphere contribution, G_j^{HS}, is determined as [37]:

$$\frac{G_j^{HS}}{RT} = -\ln(1-\eta) + 3D\frac{\eta}{1-\eta} + 3D^2\left(\frac{\eta}{(1-\eta)^2} + \frac{\eta}{(1-\eta)} + \ln(1-\eta)\right)$$
$$-D^3\left(\frac{3\eta^3-6\eta^2+\beta\eta}{(1-\eta)^3} + 2\ln(1-\eta)\right), \quad (5.20)$$

where R is the molar gas constant = 8.3145 J K^{-1} mol^{-1}, $\eta = \pi N_A \rho \sigma_w^3/6$, ρ is the molecular density, $D = \sigma_i/\sigma_w$, N_A is the Avogadro number, $\beta = 1/(kT)$ where k is the Boltzmann constant = 1.3806 10^{-23} J K^{-1}. The mean spherical approximation (MSA) for an ion-dipole interaction was determined as [38]:

$$\frac{G_j^{ID}}{RT} = -N_A e^2 z_j^2 \frac{(1-1/\varepsilon)}{\sigma_j + \sigma_w(\beta_6/\beta_3)}, \quad (5.21)$$

where z_i is the charge number of the ionic species, e is the elementary charge = 1.602 10^{-19} C, ε is the permittivity of the pure solvent. ε is related to β_6 and β_3 through the well-known Wertheim equation given as [39]:

$$\varepsilon = \frac{\beta_{12}^4\beta_3^2}{\beta_6^6} = \frac{(1+b_2/12)^4(1+b_2/3)^2}{(1-b_2/6)^6}, \quad (5.22)$$

where b_2 is a parameter from MSA theory. The dipole-dipole electrostatic term, $G^{DD}{}_j$, is calculated as [34, 40]:

$$\frac{G_j^{DD}}{RT} = \frac{-8N_A p_j^2(\varepsilon-1)}{2\sigma_w^3\left(1-\frac{\beta_{12}}{\beta_3}\right)\left(\frac{\beta_{12}}{\beta_6}\right)^3 + 2\varepsilon\left(\sigma_j+\sigma_w\frac{\beta_6}{\beta_3}\right)^3 + \left(\sigma_j+\sigma_w\frac{\beta_{12}}{\beta_6}\right)^3}, \quad (5.23)$$

where p_j, is the last fitting parameter. The Gibbs energy contribution due to the change in the standard state density is given as [35]:

$$\frac{G_j^{SS}}{RT} = -RTln(\rho RT/P^*) \,, \tag{5.24}$$

where P^* = 1 bar is the pressure of the ideal gas reference state. Lastly, the Gibbs energy that counts on the difference between unit mol fraction and unit molality reference states is given as [35]:

$$\frac{G_j^{MS}}{RT} = -RTln(M_s/b^0) \,, \tag{5.25}$$

where M_s is the molar mass of the solvent with units of kg/mol. **Eqs. 5.20 – 5.25** are the MST-based equations and reference state conversion factors contained within the summation terms in **Eq. 5.19**. With values for the five fitted parameters as well as the standard partial molar Gibbs and entropy values at the reference state for an aqueous species, **Eq. 5.19** can be used to reliably predict the apparent Gibbs energy of an aqueous species in HTHP conditions. If coupled with solid phase standard Gibbs energy values, such as **Eq. 5.5**, these values can be used to determine solubility limits for HTHP conditions. Model parameters and thermodynamic properties at the reference temperature and pressure have been previously obtained for 10 aqueous species and are presented in Tables 5.2 and 5.3 [23, 24].

Table 5.2. Fitted parameters for the MST-based thermodynamic model.

Species	A_j / a	σ_j / b	σ_w / b	p_j / c	C_j / d
Cl^-(aq)	2.336	2.999	1.372	0.000	-73.78
HCl^0(aq)	0.918	0.807	0.155	1.080	-326.81
K^+(aq)	0.615	5.284	1.122	0.000	-0.19

KCl^0(aq)	-3.499	2.999	1.372	35.637	-93.91
Na^+(aq)	-0.317	5.053	1.235	0.000	35.65
$NaOH^0$(aq)	-2.336	5.649	2.415	22.820	-74.99
NH_3^0(aq)	2.421	2.412	1.423	1.470	75.55
NH_4^+(aq)	1.449	5.316	1.022	0.000	53.05
OH^-(aq)	0.299	2.693	2.179	0.000	-89.08
SiO_2^0(aq)	2.188	1.184	2.624	1.337	-28.68

Units: a = J / (mol bar), b = Å, c = Debye, d = J / (mol K)

Table 5.3. Reference state values and charge number for the species presented in Table 5.2.

Species	$G^0_j(T_r, P_r)$/ e	$S_j^0(T_r, P_r)$/ d	z_j
Cl^-(aq)	-131290	56.74	-1
HCl^0(aq)	-134359	123.56	0
K^+(aq)	-282462	101.04	1
KCl^0 (aq)	-416338	94.31	0
Na^+(aq)	-261881	58.41	1
$NaOH^0$ (aq)	-421915	14.55	0
NH_3^0(aq)	-26706	107.82	0
NH_4^+(aq)	-79454	111.17	1
OH^-(aq)	-157297	-10.71	-1
SiO_2^0(aq)	-833411	56.48	0

Units: d = J / (mol K), e = J / mol

HTHP solubility and association constant predictions were compared to experimental data for minerals that had experimental data available in the range of conditions where the HKF

model was known to fail. Quartz solubility comparisons were made between experimental and theoretical values ranging from 150 - 500 °C for pressures of 1 - 1500 bar [31,32]. Agreement within a few percent was obtained across this range with solubility values varying from 1 x 10^{-3} to 30 x 10^{-3} mol kg^{-1} [26]. Ammonia, hydrochloric acid, potassium chloride and sodium hydroxide association constants were within 10 % of available experimental data up to 500 °C and 2000 bar [31]. Similarly, aluminum oxide and hydroxides (corundum and boehmite) systems were analyzed for a range of temperatures from 25 - 600 °C with pressures from 1 - 1000 bar [36]. Agreement in HTHP conditions was obtained between experimental values [33] and these predictions [28] for temperatures from 300 – 600 °C at a pressure of 1000 bar that were within the experimental uncertainty of ± 25 %. The solubility values obtained for these HTHP conditions ranged from 10 to 100 μmol kg^{-1} depending on temperature and pressure [36,41].

5.6 Barite Solubility Models for High Temperatures and Pressures

The MST-based model presented here was used to predict the solubility of barite in water for a wide range of temperatures and pressures. The use of this approach aims to address two issues: (1) a lack of ion pair Gibbs energy values that reliably predicts barite solubility for available experimental data, and (2) a thermodynamic model valid for petroleum and hydrothermal systems not coverable by the HKF model which are relevant to energy applications. The needed model parameters were obtained by fitting known apparent Gibbs energy values for Ba^{2+}(aq) and SO_4^{2-}(aq). Following our previous approach for adapting available HKF model species to our MST-based model [31], values from 0 - 300 °C with pressures from 1 - 250 bar were used to determine the model parameters. These range of conditions were used because the ions covered by the HKF model were clearly defined in this region [31]. The limited amount of data available to fit $BaSO_4^0$(aq) required us to use the

same approach we used to fit other species with limited influence at ambient conditions such as HCl^0(aq), KCl^0(aq) and $NaOH^0$(aq) [31]. Briefly, all the experimental solubility data available at high temperatures [28,29], where the effect of the ion-pair is expected to be most pronounced, were used to fit the standard Gibbs energy values of $BaSO_4^0$(aq). The values provided by Djamali et al., 2016 and others [16,19,20] dramatically overestimated the solubility of barite if combined with accepted Gibbs energy values from the SUPCRT92 database, so the ion pair dataset from the OLI Systems database was used as it best fit experimental data while using ions from the internally consistent SUPCRT database. These values were then fit to obtain the necessary model parameters. The obtained model parameters for these species are presented in Table 5.4 and the reference thermodynamic properties are given in Table 5.5.

Table 5.4. Fitted parameters needed to predict barite solubility using the MST-based thermodynamic model.

Species	A_j / a	σ_j / b	σ_w / b	p_j / c	C_j / d
Ba^{2+}(aq)	-1.941	7.782	0.924	0.000	-63.85
SO_4^{2-}(aq)	2.113	5.206	1.728	0.000	-167.53
$BaSO_4^0$(aq)	-16.887	1.670	3.478	1.040	-75.40
Units: a = J/(mol bar), b = Å, c = Debye, d = J/(mol K)					

Table 5.5. Reference state values and charge number for the species presented in Table 5.4.

Species	$G^0_j(T_r, P_r)$/ e	$S_j^0(T_r, P_r)$/ d	z_j
Ba^{2+}(aq)	-560782	9.62	2
SO_4^{2-}(aq)	-744459	18.83	-2

$BaSO_4^0$(aq)	-1290320	33.30	0

Units: d = J/(mol K), e = J / mol

Significantly better agreement was obtained between the experimental data and the new model predictions relative to model predictions by Ref. [16], Ref. [15] and OLI Systems. OLI Systems predictions were shown as their predictions were the second closest to capturing the solubility trends. Barite solubility values from experimental measurements and model predictions are presented in Figure 5.4 and Figure 5.5.

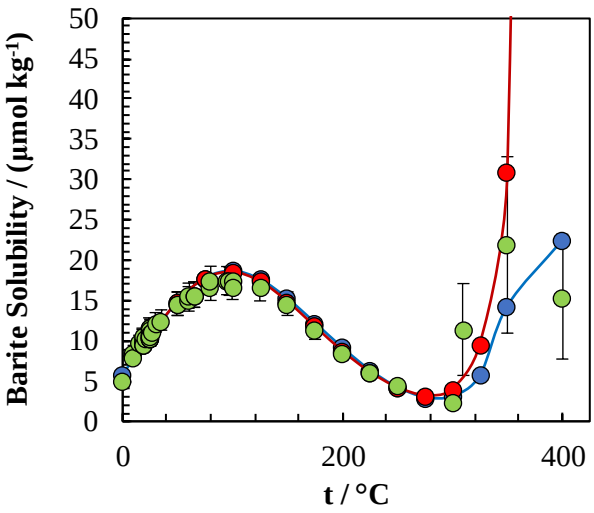

Figure 5.4: Barite solubility comparisons for P_{sat} then 500 bar at 400 °C. (● = experimental data [15,28], ● = this work, ● = OLI Systems)

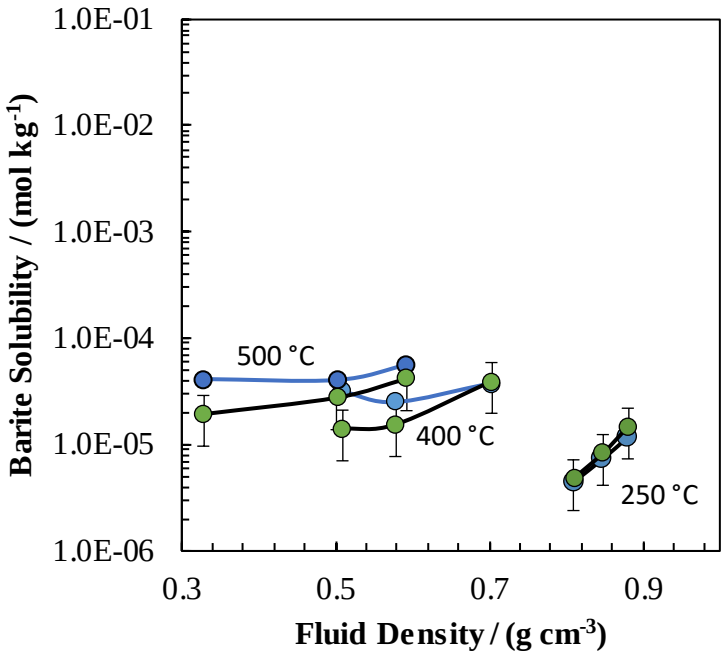

Figure 5.5: Barite solubility comparisons between the MST model and experimental data for HTHP conditions. (● = experimental data [28,29], ● = this work)

As temperatures increased above 300 °C, the dominant barium-containing species switched from $Ba^{2+}(aq)$ to $BaSO_4^0(aq)$. In general, though the trend in solubility varies considerably with temperature, the new model was able to follow the available data with an accuracy within experimental uncertainty. This is particularly true because the available data sets contained large uncertainties (> 20 %), in addition to some sizable disagreements between sets (>200 %). Table 5.6 – Table 5.8 provide data from the MST model for the conditions examined.

Table 5.6. Standard apparent partial molar Gibbs energy values from the MST-based models.

t / °C	P / bar	$BaSO_4^0(aq)$ / kJ mol^{-1}	$Ba^{2+}(aq)$ / kJ mol^{-1}	$SO_4^{2-}(aq)$ / kJ mol^{-1}	$BaSO_4(s)$ / kJ mol^{-1}
0	1.0	-1290.59	-560.49	-743.70	-1358.89

25	1.0	-1290.31	-560.78	-744.46	-1362.09
50	1.0	-1292.06	-561.01	-744.76	-1365.50
75	1.0	-1295.16	-561.16	-744.65	-1369.12
100	1.0	-1299.30	-561.24	-744.14	-1372.94
125	2.3	-1304.17	-561.24	-743.24	-1376.95
150	4.8	-1309.57	-561.18	-741.92	-1381.14
175	8.9	-1315.35	-561.03	-740.18	-1385.50
200	15.5	-1321.37	-560.78	-737.93	-1390.02
225	25.5	-1327.57	-560.40	-735.08	-1394.68
250	39.7	-1333.94	-559.82	-731.47	-1399.49
275	59.4	-1340.48	-558.94	-726.80	-1404.42
300	85.8	-1347.22	-557.48	-720.49	-1409.46
325	120.0	-1354.29	-554.88	-711.33	-1414.61
350	163.4	-1362.03	-549.22	-695.48	-1419.83
400	500	-1369.50	-546.03	-687.07	-1429.40

Table 5.7. Standard apparent partial molar Gibbs energy values from the MST-based model for HTHP conditions.

t / °C	P / bar	$BaSO_4^0$(aq) / kJ mol^{-1}	Ba^{2+}(aq) / kJ mol^{-1}	SO_4^{2-}(aq) / kJ mol^{-1}	$BaSO_4$(s) / kJ mol^{-1}
189	404	-1321.38	-561.25	-738.93	-1385.97
190	904	-1323.33	-561.83	-738.73	-1383.54
247	92	-1334.14	-559.74	-731.73	-1398.62
248	522	-1335.37	-560.32	-732.89	-1396.42
249	1010	-1337.18	-560.91	-733.37	-1394.23
279	996	-1344.38	-560.31	-729.90	-1400.36

310	99	-1349.95	-555.99	-716.18	-1411.51
350	171	-1361.27	-548.28	-694.26	-1419.80
400	382	-1371.52	-537.70	-669.59	-1430.02
400	500	-1369.50	-546.03	-687.07	-1429.40
400	1070	-1368.95	-554.38	-706.93	-1426.43
400	2100	-1373.55	-557.91	-714.74	-1421.07
500	586	-1388.76	-477.61	-561.64	-1453.04
500	914	-1385.72	-531.00	-651.62	-1451.33
500	1276	-1385.79	-543.39	-676.13	-1449.44
600	874	-1398.50	-467.58	-539.75	-1477.38
600	1084	-1398.17	-499.85	-591.16	-1476.28

Table 5.8. Comparison of MST-based model predictions to available experimental data [15,28].

t / °C	P / bar	$b_{s,model}$ / µmol kg^{-1}	$b_{s,exp}$ / µmol kg^{-1}
0	1	5.88	5.18
25	1	10.47	11.10
50	1	14.89	14.81
75	1	17.82	16.65
100	1.0	18.68	16.93
125	2.3	17.63	15.98
150	4.8	15.25	14.14
175	8.9	12.24	11.71
200	15.5	9.14	9.04
225	25.5	6.38	6.44

250	39.7	4.25	4.24
275	59.4	3.02	2.77
300	85.8	3.14	2.35
325	120.0	5.73	3.30
350	163.4	14.33	21.90
400	500	22.48	15.45

The considerable disagreements between measurements suggest that there are likely errors within one or more of the studies for this system. As such, the reliability of our predictions can be further verified if more experimental data were to become available to help us discern which sets best represent this system.

5.7 Section Summary

Scaling and mineral precipitation in produced waters is a problem that plagues the oil, natural gas and high enthalpy geothermal community. A thermodynamic analysis of the barite-water system provides a means to predict if a mineral will be dissolved or precipitated in a wide range of conditions. Predominance diagrams and speciation models provide a means to understand how changes in solution composition impact mineral behavior for a given system. At ambient conditions, increases in pH above 2 increases the solubility of barite from ~1 to 10 μmol kg^{-1}, but further increases to pH beyond 5 had little effect. As temperature increases, the solubility of barite in pure water increases to about 17 μmol kg^{-1} but then decreases to about 5 μmol kg^{-1} by 300 °C at saturated pressures. Available HTHP data indicate that the solubility increases at higher temperatures and pressures again to 10s of μmol kg^{-1} at temperatures > 300 °C. Data available indicates that the $BaSO_4^0$(aq) ion pair plays a key role in governing the solubility limit at HTHP conditions. Therefore, a new MST-based model was extended to provide reliable predictions of barite solubility for a wide range of conditions by providing $BaSO_4^0$(aq), Ba^{2+}(aq) and SO_4^{2-}(aq) Gibbs energy values in HTHP conditions.

5.8 List of Figures

5.9 List of Tables

5.10 Nomenclature

Symbol	Units	Name
a_i	unitless	Species activity
A_i	J mol^{-1} Pa^{-1}	Empirical short-range interaction parameter
b_i	mol kg^{-1}	Species concentration, molality
b^0	mol/kg	Standard molality
b_2	unitless	Dipole-dipole interaction parameter from MSA theory
C_i	J mol^{-1} K^{-1}	Empirical short-range interaction parameter
D	unitless	(σ_i/σ_w), ratio of diameters
e	C	Elementary charge of an electron
$\Delta_f G^0$	J mol^{-1}	Standard Gibbs energy of formation
$\Delta_r G^0$	J mol^{-1}	Standard Gibbs energy of reaction
$\Delta G^0_i(T, P)$	J mol^{-1}	Apparent standard partial molar Gibbs energy
$\Delta_f G^0_j(T_r,P_r)$	J mol^{-1}	Reference standard partial molar Gibbs energy of formation
$G^0_i(T, P)$	J mol^{-1}	Standard partial molar Gibbs energy
$G^0_j(T_r, P_r)$	J mol^{-1}	Reference standard partial molar Gibbs energy
$G_j^k(T_r,P_r)$	J mol^{-1}	Reference molecular statistical Gibbs energy contribution
$G_j^k(T, P)$	J mol^{-1}	Molecular statistical Gibbs energy contribution
G_j^{HS}	J mol^{-1}	Hard sphere Gibbs energy contribution
G_j^{ID}	J mol^{-1}	Ion-dipole Gibbs energy contribution
G_j^{DD}	J mol^{-1}	Dipole-dipole Gibbs energy contribution
G_j^{SS}	J mol^{-1}	Standard state solution density Gibbs energy contribution
G_j^{MS}	J mol^{-1}	Standard state unit molality Gibbs energy contribution
K	J K^{-1}	Boltzmann's constant
IAP	unitless	Ion activity product
K_{eq}	unitless	Equilibrium constant
K_{sp}	unitless	Solubility product constant
M_s	kg mol^{-1}	Molar mass of solvent
N_A	mol^{-1}	Avogadro's number
P_r	Pa	Reference pressure
P^*	Pa	Ideal gas reference state pressure
P	Pa	Pressure
p_i	C m	MST model parameter, solute dipole moment
R	J mol^{-1} K^{-1}	Molar gas constant
SI	unitless	Scaling index
$S^0_j(T_r,P_r)$	J mol^{-1} K^{-1}	Reference standard partial molar entropy
$S_j^k(T_r, P_r)$	J mol^{-1} K^{-1}	Reference molecular statistical entropy contribution
T_r	K	Reference temperature
T	K	Thermodynamic temperature
T	°C	Temperature
z_i	unitless	Charge number of an ion
α_0	mol kg^{-1}	Empirical parameter, barite solubility equation
α_1	mol kg^{-1}° C^{-1}	Empirical parameter, barite solubility equation
α_2	mol kg^{-1} °C^{-2}	Empirical parameter, barite solubility equation
α_3	mol kg^{-1} °C^{-3}	Empirical parameter, barite solubility equation
$\beta = 1/kT$	J^{-1}	Thermodynamic beta, MST theory
β_3	unitless	($1+b_2/3$), Wertheim equation parameter
β_6	unitless	($1-b_2/6$),Wertheim equation parameter

β_{12}	unitless	$(1+b_2/12)$, Wertheim equation parameter
γ_i	unitless	Species activity coefficient
ε	unitless	Permittivity of water
η	unitless	$(\pi\sigma_w^3 n/6)$, Hard sphere equation parameter
ρ	kg m^{-3}	Density of water
σ_j	m	MST model parameter, solute diameter
σ_w	m	MST model parameter, solvent diameter
Ω	unitless	Scaling tendency

References

[1] OLI Systems, OLI Studio Stream Analyzer User Guide. V 9.5, n.d.

[2] M. Brown, Full Scale Attack, Review. 30 (1998) 30–32.

[3] M. Amiri, J. Moghadasi, The Effect of Temperature on Calcium Carbonate Scale Formation in Iranian Oil Reservoirs Using OLI ScaleChem Software, Pet. Sci. Technol. 30 (2012). doi:10.1080/10916461003735145.

[4] A.N.P. Vankeuren, J.A. Hakala, K. Jarvis, J.E. Moore, Mineral Reactions in Shale Gas Reservoirs : Barite Scale Formation from Reusing Produced Water As Hydraulic Fracturing Fluid, Environ. Sci. Technol. 51 (2017) 9391–9402. doi:10.1021/acs.est.7b01979.

[5] M.S. Kamal, I. Hussein, M. Mahmoud, A.S. Sultan, M.A.S. Saad, Oilfield scale formation and chemical removal: A review, J. Pet. Sci. Eng. 171 (2018) 127–139. doi:10.1016/j.petrol.2018.07.037.

[6] A.A. Olajire, A review of oilfield scale management technology for oil and gas production, J. Pet. Sci. Eng. 135 (2015) 723–737. doi:10.1016/j.petrol.2015.09.011.

[7] A.T. Kan, J.Z. Dai, G. Deng, G. Ruan, W. Li, K. Harouaka, Y.T. Lu, X. Wang, Y. Zhao, M.B. Tomson, Recent advances in scale prediction, approach, and limitations, Soc. Pet. Eng. - SPE Int. Oilf. Scale Conf. Exhib. 2018. (2018) 20–21. doi:10.2118/190754-pa.

[8] A.D. Jew, M.K. Dustin, A.L. Harrison, C.M. Joe-wong, D.L. Thomas, K. Maher, G.E.

Brown, J.R. Bargar, Impact of Organics and Carbonates on the Oxidation and Precipitation of Iron during Hydraulic Fracturing of Shale, Energy and Fuels. 31 (2017). doi:10.1021/acs.energyfuels.6b03220.

[9] M.K. Dustin, J.R. Bargar, A.D. Jew, A.L. Harrison, C. Joe-wong, D.L. Thomas, G.E. Brown, K. Maher, Shale Kerogen : Hydraulic Fracturing Fluid Interactions and Contaminant Release, Energy & Fuels. 32 (2018) 8966–8977. doi:10.1021/acs.energyfuels.8b01037.

[10] S. Blumsack, Production Decline for Shale Gas Wells, EME 801 Energy Mark. Policy Regul. (2021). https://www.e-education.psu.edu/eme801/node/521.

[11] Q. Li, A.D. Jew, A. Kohli, K. Maher, G.E. Brown, J.R. Bargar, Thicknesses of Chemically Altered Zones in Shale Matrices Resulting from Interactions with Hydraulic Fracturing Fluid, Energy and Fuels. 33 (2019) 6878–6889. doi:10.1021/acs.energyfuels.8b04527.

[12] E.R. Cohen, T. Cvitas, J.G. Frey, B. Holmström, K. Kuchitsu, R. Marquardt, I. Mills, F. Pavese, Quantities, Units and Symbols in Physcial Chemistry, in: IUPAC Green B., 3rd Editio, IUPAC & RSC Publishing, Cambridge, 2008: pp. 1–236.

[13] Greg Anderson, Rock-Water Systems, in: Thermodyn. Nat. Syst., Second, Cambridge University Press, Cambridge, 2005: pp. 473–497.

[14] J.W. Johnson, E.H. Oelkers, H.C. Helgeson, SUPCRT92: A software package for calculating the standard molal thermodynamic properties of minerals, gases, aqueous species, and reactions from 1 to 5000 bars and 0 to 1000˚C, Comput. Geosci. 18 (1992) 899–947.

[15] B.S. Krumgalz, Temperature Dependence of Mineral Solubility in Water. Part 3. Alkaline and Alkaline Earth Sulfates, 2018. doi:10.1063/1.5031951.

[16] E. Djamali, W.G. Chapman, K.R. Cox, A Systematic Investigation of the

Thermodynamic Properties of Aqueous Barium Sulfate up to High Temperatures and High Pressures, J. Chem. Eng. Data. 61 (2016) 3585–3594. doi:10.1021/acs.jced.6b00506.

[17] B. Johnson, L. Kanagy, J. Rodgers, J. Castle, Chemical, Physical, and Risk Characterization of Natural Gas Storage Produced Waters, Water, Air Soil Pollut. 191 (2008) 33–54.

[18] S.N. Lvov, N.N. Akinfiev, A. V. Bandura, F. Sigon, G. Perboni, Multisys: Computer Code for Calculating Multicomponent Equilibria in High-Temperature Subcritical and Supercritical Aqueous Systems, in: P.R. Tremaine, P.G. Hill, D.E. Irish, P. V. Palakrishnan (Eds.), Steam, Water, Hydrothermal Syst. Phys. Chem. Meet. Needs Ind., NRC Press, Ottawa, 2000: pp. 866–873.

[19] C. Monnin, A thermodynamic model for the solubility of barite and celestite in electrolyte solutions and seawater to 200°C and to 1 kbar, Chem. Geol. 153 (1999) 187–209. doi:10.1016/S0009-2541(98)00171-5.

[20] A.R. Felmy, D. Rai, J.E. Amonette, The solubility of barite and celestite in sodium sulfate: Evaluation of thermodynamic data, J. Solution Chem. 19 (1990) 175–185. doi:10.1007/BF00646611.

[21] S.N. Lvov, Introduction to Electrochemical Science and Engineering, 1st ed., CRC press Inc, Boca Raton, FL, 2014.

[22] D.M. Hall, J.R. Beck, E. Brand, M. Ziomek-Moroz, S.N. Lvov, Copper-Copper Sulfate Reference Electrode for Operating in High Temperature and High Pressure Aqueous Environments, Electrochim. Acta. 221 (2016) 96–106. doi:10.1016/j.electacta.2016.10.143.

[23] D.M. Hall, N.N. Akinfiev, E.G. LaRow, R.S. Schatz, S.N. Lvov, Thermodynamics and Efficiency of a CuCl(aq)/HCl(aq) Electrolyzer, Electrochim. Acta. 143 (2014) 70–82.

doi:10.1016/j.electacta.2014.08.018.

[24] R. Feng, J. Beck, D.M. Hall, A. Buyuksagis, M. Ziomek-Moroz, S.N. Lvov, Effects of CO2 and H2S on Corrosion of Martensitic Steels in Brines at Low Temperature, Corrosion. 74 (2018) 276–287. doi:https://doi.org/10.5006/2406.

[25] V. Valyashko, Hydrothermal Properties of Materials, Wiley-VCH, 2008.

[26] G.W. Morey, J.M. Hesselgesser, The Solubility of Some Minerals in Superheated Steam at High Pressures, Econ. Geol. 46 (1951) 821–835.

[27] B. Strübel, Zur Kenntnis und genetischen Bedeutung des Systems BaSO4 – NaCl – H2O. (To the knowledge and genetic importance of the system BaSO4 – NaCl – H2O.), Neues Jahrbuch. Min. Mh. 7/8 (1967) 223–233.

[28] H. Gundlach, D. Stoppel, G. Strubel, The Hydrothermal Solubility of Barite, Proc. 24th Intern. Geol. Congr. 10 (1972) 291–229.

[29] C.. Blount, Barite solubilities and thermodynamic quantities up to 300 °C and 1400 bars, Amer. Mineral. 62 (1977) 942–957.

[30] F.W.. Dickson, C.W.. Blount, G. Tunell, Use of hydrothermal solution equipment to determine the solubility of anhydrite in water from 100°C to 275°C and from 1 bar to 1,000 bars pressure, Amer. J. Sci. 261 (1963) 61–78.

[31] S.N. Lvov, D.M. Hall, A. V. Bandura, I.K. Gamwo, A semi-empirical molecular statistical thermodynamic model for calculating standard molar Gibbs energies of aqueous species above and below the critical point of water, J. Mol. Liq. 270 (2018) 62–73. doi:10.1016/j.molliq.2018.01.074.

[32] S.N. Lvov, D.M. Hall, I.K. Gamwo, Molecular Statistical Thermodynamics to Model Quartz Solubility in Ultra High-Enthalpy Geothermal Systems, in: 4th Annu. Int. Conf. Geol. Earth Sci. (GEOS 2015), Global Science and Technology Forum (GSTF), 2015. doi:10.5176/2251-3353_GEOS15.44.

[33] T. Phi, R. Elgaddafi, M. Al Ramadan, K. Fahd, R. Ahmed, C. Teodoriu, Well integrity issues: Extreme high-pressure high-temperature wells and geothermal wells a review, Soc. Pet. Eng. - SPE Therm. Well Integr. Des. Symp. 2019, TWID 2019. (2019). doi:10.2118/198687-ms.

[34] A. V. Bandura, M.F. Holovko, S.N. Lvov, The chemical potential of a dipole in dipolar solvent at infinite dilution: Mean spherical approximation and Monte Carlo simulation, J. Mol. Liq. 270 (2018) 52–61. doi:10.1016/j.molliq.2018.01.015.

[35] S.N. Lvov, V.A. Umniashkin, A. Sharygin, M.F. Holovko, The molecular statistical theory of infinitely dilute solutions based on the ion-dipole model with Lennard-Jones interaction, Fluid Phase Equilib. 58 (1990) 283–305. doi:10.1016/0378-3812(90)85137-Y.

[36] S.N. Lvov, D.D. Macdonald, Thermodynamic computer simulation of hydrothermal synthesis of oxides in supercritical aqueous environments, in: K.E. Spear (Ed.), High Temp. Mater. Chem., Electrochemical Society, Pennington, 1997: pp. 472–479.

[37] G.A. Mansoori, N.F. Carnahan, K.E. Starling, T.W. Leland Jr., Equilibrium Thermodynamic Properties of the Mixture of Hard Spheres, J. Chem. Phys. 54 (1971) 1523–1525. doi:10.1063/1.1675048.

[38] L. Blum, F. Vericat, W.R. Fawcett, On the Mean Spherical approximation for hard ions and dipoles, J. Chem. Phys. 96 (1992).

[39] M.S. Wertheim, Exact Solution of the Mean Spherical Model for Fluids of Hard Spheres with Permanent Electric Dipole Moments, J. Chem. Phys. 55 (1971) 4291. doi:10.1063/1.1676751.

[40] R. Richert, Solvation energy of ions and dipoles in a finite number of solvent shells, J. Phys. Condens. Matter. 8 (1996) 6185–6190. doi:10.1088/0953-8984/8/34/008.

[41] K.V. Ragnarsdóttir, J. V. Walther, Experimental determination of corundum

solubilities in pure water between 400-700°C and 1-3 kbar, Geochim. Cosmochim. Acta. 49 (1985) 2109–2115. doi:10.1016/0016-7037(85)90068-7.